Available online at www.sciencedirect.com
ScienceDirect
Trans. Nonferrous Met. Soc. China 32(2022) 972−979
Transactions of Nonferrous Metals Society of China
www.tnmsc.cn

Microstructure and magnetic properties of FeAs with coarse-grain and nanocrystalline structure

Yuan ZHOU[1], Yun-yan WANG[1,2], Yan-jie LIANG[1,2], Yi-wei ZHOU[1], Zhen-xing LIU[1], Cong PENG[1,2], Yong KE[1,2], Xiao-bo MIN[1,2]

1. School of Metallurgy and Environment, Central South University, Changsha 410083, China;
2. Chinese National Engineering Research Center for Control & Treatment of Heavy Metal Pollution, Changsha 410083, China

Received 4 February 2021; accepted 24 November 2021

Abstract: The microstructure and magnetic properties of iron arsenide (FeAs) with coarse-grain and nanocrystalline structure were investigated. Coarse-grain FeAs was synthesized through high-energy ball milling and heat treatment. Nanocrystalline FeAs was obtained by ball milling of coarse-grain FeAs. The results suggest that the reduced grain size of FeAs (from >100 to 32.4 nm) is accompanied by the introduction of internal strains up to 0.568% with ball milling time from 0 to 32 h. The magnetic properties of FeAs show that the coercivity is reduced from 29.2 to 15.6 kA/m and the magnetization is increased over time of milling. The low coercivity is mainly due to the small grain size stemmed from ball milling, while the increase of magnetization is primarily caused by the change of lattice parameters of FeAs and the emergence of superparamagnetic phase at the same time.

Key words: high-energy ball milling; iron arsenide; coercivity; magnetization

1 Introduction

The special magnetic characteristics of FeAs were noticed firstly in superconducting materials. The iron-based layered compounds ReOFeAs (Re=La, Sm, Nd, Ce, Gd) have been reported to exhibit superconducting phases with relatively high transition temperature [1−3]. Series of ReOFeAs crystals are composed of a stack of alternating ReO and FeAs layers, while the edge shared $FeAs_4$ tetrahedron contained in FeAs layer plays key role in superconductivity [4,5].

In addition to superconductors, iron mono-arsenide FeAs has potential application in spintronic and magnetic devices with control over morphology, composition and structure [6]. With MnP type structure, FeAs has cooperative magnetism which belongs to the helimagnetic class. This magnetic behavior of FeAs is a consequence of its atomic arrangement, especially the geometry of the metal atom sublattice [7]. In the unit cell of FeAs structure, each Fe atom is coordinated by six As atoms, forming distorted octahedron. The FeAs can be refined in the *Pnma* and $Pna2_1$ space group while the latter one has a lower symmetry [8]. The Mössbauer spectra of single crystal FeAs suggest a competition between highly directional covalent Fe−As−Fe and metallic bonds [9].

In earlier researches, bulk FeAs and FeAs nanoparticles have been synthesized and studied. The bulk FeAs crystallized in the orthorhombic MnP type structure has lattice parameters of a=5.4420(7) Å, b=3.3727(6) Å and c=6.0278(7) Å at room temperature by X-ray diffraction [10] while the neutron diffraction measurements show

Corresponding author: Yan-jie LIANG, Tel: +86-13787042003, E-mail: LiangyanjieCSU@163.com
DOI: 10.1016/S1003-6326(22)65847-3

significant difference in analytical structure as b= 3.325(1) Å when the temperature was 12 K [11]. JEFFRIES et al [12] investigated the structure and electrical transport properties of FeAs and found that the MnP type structure could persist for up to 25 GPa. FeAs with polycrystalline structures have both antiferromagnetic properties with T_N of ~70 K. According to polarized neutron measurements, the non collinear "helical" magnetic order at T_N=77 K with magnetic moment along b-direction is higher than that along the a-direction [13]. With regard to FeAs nanoparticles, the magnetic characterization of the carbonaceous shell-coating FeAs with the size in the range of 8−10 nm revealed the superparamagnetic nature of FeAs with irreversibility temperature T_{irr} =71 K and blocking temperature T_B=63 K in applied magnetic field strength H=79.6 kA/m [6]. Except for the bulk FeAs and FeAs nanoparticles isolated by amorphous carbon, microstructure and magnetic properties of FeAs particles composed by nanoscale grains are almost completely lacking.

Materials with nanostructure have been studied in the last decade due to their unusual properties that are normally attributed to the ultrafine grains, changed lattice parameters and large amounts of grain boundaries [14−16]. It is found that the coercivity decreases from 15.8 to 1.8 A/m when the grain size of α-Fe nanocrystallites is reduced from 13.2 to 7.3 nm in $Fe_{86}Zr_7B_6Cu_1$ ribbons [17]. MAHDAVI and ALLAHKARAM [18] showed that the decreased crystallite size of cobalt films could increase their microhardness without significant effect on current efficiency. Therefore, an investigation of nanocrystalline FeAs and comprehension of the correlation between microstructure and magnetic properties can help understand and optimize the magnetic properties of FeAs and similar materials.

In this work, new synthesis routes of coarse-grain and nanocrystalline FeAs were provided and their microstructure and magnetic properties were investigated. To explore the effects of mechanical force induced by ball milling on the microstructure and magnetic properties of FeAs, nanocrystalline FeAs with different milling time was also studied.

2 Experimental

The synthesis of coarse-grain FeAs was processed by high-energy ball milling and heat treatment, followed by acid-washing purification. In the ball milling synthesis stage, the stoichiometric Fe (99.5%) and As (99.0%) powders were sealed and milled in a 500 mL stainless-steel vial and mixed with ZrO_2 balls. The ball-to-powder mass ratio was 20:1, and the vial rotation speed was 320 r/min. The vial was equipped with two vent holes and the Ar purge was conducted for three times before ball milling. The milling time ranged from 0 to 40 h to obtain alloyed FeAs. Subsequently, the impurity components in the prepared FeAs powder were removed by heat treatment at 750 °C and HCl solution pickling. During the heat treatment, the samples were loaded in tube furnace with Ar purge, heated up to 750 °C, kept at this temperature for 24 h and slowly cooled down to ambient conditions. During the HCl solution pickling, samples were mixed with 1 mol HCl solution in solid-to-liquid ratio (1:20 g/mL), vibrated for 24 h at room temperature, and finally washed with water and drying.

In the synthesis route of nanocrystalline FeAs, the mechanically alloyed FeAs in the first stage was loaded in a ZrO_2 vial and mixed with ZrO_2 balls of 10 mm in diameter. The vial was equipped with two vent holes and the Ar purge was conducted for three times before ball milling. To avoid the local temperature rise inside the vials, the milling cycle was set to be 45 min of milling at 320 r/min followed by a pause of 15 min. The samples were milled at intervals from 8 to 32 h.

The structural evolution and phase transformation were investigated by X-ray diffraction (XRD), using Rigaku TTR III diffractometer equipped with Cu K_α radiation (λ= 0.154056 nm). The measurements were performed in steps of 0.01°, with 1 s per step at room temperature. The microstructural and structural parameters were deduced from Rietveld refinement of the XRD patterns using the Fullprof program. The full width at half maxima (FWHM) of all samples has been calculated by using Voigt function (convolution of Gaussian and Lorentzian function) and grain sizes have been estimated by Debye−Scherrer formula. Morphological and microstructural changes of the powder particles during the milling process were followed by scanning electron microscopy (SEM) in a Nova NanoSEM 230 equipment and transmission electron

microscopy (TEM) in a Tecnai G2 20S-Twin. Samples for SEM were prepared by spreading a small amount of powder on a sticky conductive tape. Samples for TEM were made by dispersing FeAs particles in ethanol followed by ultrasonication. ^{57}Fe Mössbauer spectroscopy was carried out in the standard transmission geometry in WissEL Mössbauer Spectrometer at room temperature, using a conventional constant acceleration drive and γ-ray source of ^{57}Co in Rh-matrix. The spectra were fitted with a least-square method [19].

Magnetic properties were collected from the vibrating sample magnetometer (VSM) option of physical property measurement system (PPMS). The M–H hysteresis loops were performed in external magnetic field between −2 and 2 T at 77 K. Thermomagnetic curves were composed of two parts: the zero-field cooled (ZFC) data were obtained after the cooling process without applied magnetic field and then measuring the magnetization in temperature rising process by applying a magnetic field strength of 79.6 kA/m with 4 K/min temperature increase; the field-cooled (FC) data were collected after cooling down under magnetic field strength of 79.6 kA/m and temperature decreasing rate of 4 K/min.

3 Results and discussion

3.1 Coarse-grain FeAs synthesized by high-energy ball milling

Figure 1 displays the evolution of the XRD patterns for the synthesis process of FeAs by high-energy ball milling. The results show that the elemental As and Fe can generate FeAs under high-energy mechanical force. After milling for 16 h, the peaks of Fe remain unchanged while most diffraction peaks of arsenic disappear and the strongest characteristic peak shows distinct broadening and weakening, indicating the amorphization of As. Dramatic changes of phase are observed after milling for 40 h, where the characteristic peaks of Fe (2θ=44.67° and 65.02°) disappear and the FeAs peaks become dominant.

Some impurity phases, $FeAs_2$ and As_2O_3, can be found in the mechanically alloyed FeAs. However, all of the impurities can be removed by subsequent heat treatment and acid washing. As shown in Fig. 1(d), only characteristic peaks of FeAs can be observed in XRD pattern after purification. Moreover, the characteristic peaks of XRD become higher, which indicates that the subsequent purification can not only reduce the impurity content but also optimize the quality of the FeAs crystal. As shown in Fig. 2, the FeAs particles are characterized by uneven shape and inconspicuous coalescence, with sizes mostly between 1 and 5 μm. As shown in the local enlarged image in Fig. 2, there are small holes on the surface of the particles, which may be caused by the volatilization of unreacted elemental arsenic during heat treatment. Hence, FeAs with high crystallinity is obtained by high-energy ball milling followed by purification.

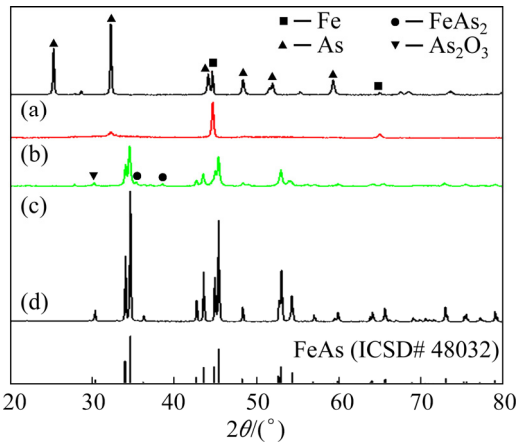

Fig. 1 XRD patterns of synthesis process of FeAs: (a) Original mixture of Fe and As powders; (b, c) High-energy ball-milled samples for 16 and 40 h, respectively; (d) FeAs after heat and acid treatment

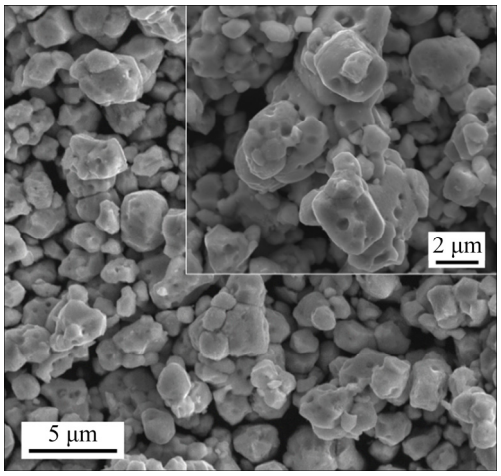

Fig. 2 SEM image of FeAs with high crystallinity

3.2 Microstructure of nanocrystalline FeAs

Compared with the well-crystallized FeAs, some nanocrystalline or amorphous samples may have better magnetic properties [20−22]. Therefore,

high-energy ball milling is used to refine and modify the mechanically alloyed FeAs with high crystallinity. Figure 3 shows the XRD patterns for structural evolution of FeAs with time of the ball milling. Only one phase is observed in XRD patterns of all samples, consistent with the orthorhombic FeAs (ICSD# 48032). With the milling time increasing, all characteristic peaks of FeAs show persistent broadening of shape and weakening of intensity, suggesting the decrease of grain size and increase of internal strain [23]. The regular change of grain size is caused by the large number of dislocations generated by ball milling [22]. Along with the increase of dislocation density, the FeAs crystals decompose into smaller grains.

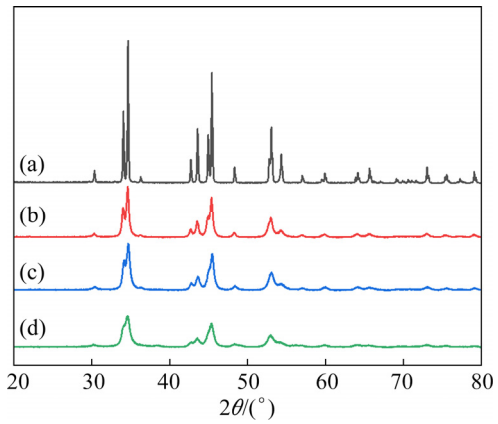

Fig. 3 XRD patterns of FeAs powders with different milling time: (a) 0 h; (b) 8 h; (c) 16 h; (d) 32 h

Details for structural analysis of mechanically milled FeAs particles such as lattice parameters, grain sizes, and internal strains were obtained using the Rietveld structure refinement method [24] and the results are given in Table 1. The refined grain sizes decrease below 100 nm and reach about 32.4 nm when the milling time comes up to 32 h. Meanwhile, the internal strain increases from 0 to 0.568% under continuous mechanical force. With increasing the milling time, the refined lattice parameters also show regular increases especially for lattice constant *b*. The changes of lattice parameters are in excellent agreement with previously reported study of the effect of thermal expansion on those of bulk FeAs [11]. Given the interplanar spacings, it is a matter of course that the *b* axis has a preferential contraction and expansion. The regular changes in lattice parameters affect the magnetic properties.

Table 1 Refined lattice parameters for mechanically milled FeAs particles

Milling time/h	Lattice constant/nm			Grain size/nm	Internal strain/%
	a	*b*	*c*		
0	5.4341	3.3778	6.0224	>100 nm	−
8	5.4370	3.3809	6.0252	47.9	0.209
16	5.4343	3.3842	6.0263	38.2	0.313
32	5.4370	3.3889	6.0293	32.4	0.568

All samples are refined in orthorhombic *Pnma* space group

To study the effects of mechanical modification on the surface and inside of FeAs particle, SEM and TEM images for FeAs before and after ball milling are analyzed. As shown in Figs. 4(a, b), the particle size of FeAs decreases significantly from 1−5 μm to 0.1−1 μm after ball milling. A large amount of nanoscale FeAs particles are obtained and a distinct agglomeration is observed. The TEM analysis shows that the ball milling can change the internal structure of FeAs grains. As shown in Figs. 4(c, d), FeAs before ball milling has clear lattice fringe with large area and distinct edge. The calculated result of spacing of adjacent lattice fringe exhibits an interplanar spacing of 3.01 Å for 〈020〉. After ball milling for 32 h, the grain size of FeAs is significantly reduced accompanied by a large amount of amorphous structure, which is also consistent with the XRD results.

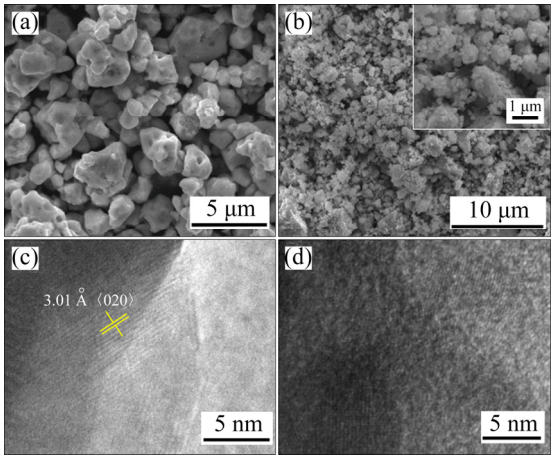

Fig. 4 SEM (a, b) and TEM (c, d) micrographs of FeAs particles before (a, c) and after ball milling for 32 h (b, d)

3.3 Magnetic properties and Mössbauer analysis

To explain the magnetic behavior of the mechanically milled FeAs particles, magnetization as a function of applied field strength (*M*−*H*) and

temperature (*M*−*T*) was investigated. Figure 5(a) exhibits a remarkable increase of magnetization in the range of 198.9−1591.5 kA/m for ball-milled FeAs particles, following the time of ball milling. As can be seen, the magnetization of FeAs increases from 1.08 to 1.85 A·m^2/kg after milling for 32 h. In order to exclude the possible effects on magnetic properties from the presence of unreacted raw Fe which cannot be detected in X-ray diffraction, the *M*−*H* curve of raw Fe powder was also investigated and the results reach saturation magnetization in applied magnetic induction around 1 T, thereby indicating a reliable magnetic data of FeAs samples. The increase of magnetization along with milling time suggests a change of the nearest neighbor circumstances of the magnetic element, namely the increase of interatomic distance between atom Fe and its nearest non-magnetic atom As, which is coherent with the change of lattice parameter.

Hysteresis loops in Figs. 5(b, c) show that the coercivity gradually decreases with milling time from 29.2 to 15.6 kA/m, and there is nearly no visible change with time of ball milling from 0 to 32 h. According to literature, grain size is one of the main factors that affect coercivity and the deduction of coercivity can be related to the lower grain size especially in ultrafine grain size materials [25]. Ball milling results in microscopic strain and many defects in the strain area, which can hinder the movement of domain walls and lead to magnetic changes. Meanwhile, for ultrafine particles, the region of amorphous phase among nanoscale grains can destroy the exchange coupling between them and therefore change the magnetism of matrix.

With regard to the *M*−*T* curve for sample without ball milling, the ZFC magnetization rises continuously from the lowest temperature to around 106 K. Then, the magnetization drops gradually until room temperature. The FC magnetization behaves similarly in high-temperature area compared with the ZFC curve, and remains almost unchanged at temperature below 106 K. The divergence of the ZFC−FC curves is a typical feature of several magnetic phenomena like superparamagnetism [26], random anisotropy [27], and spin glass behavior [28]. But, to further determine the type of magnetic behavior, solid reference or scientific proof should be provided.

It can be seen from Fig. 6 that there are two

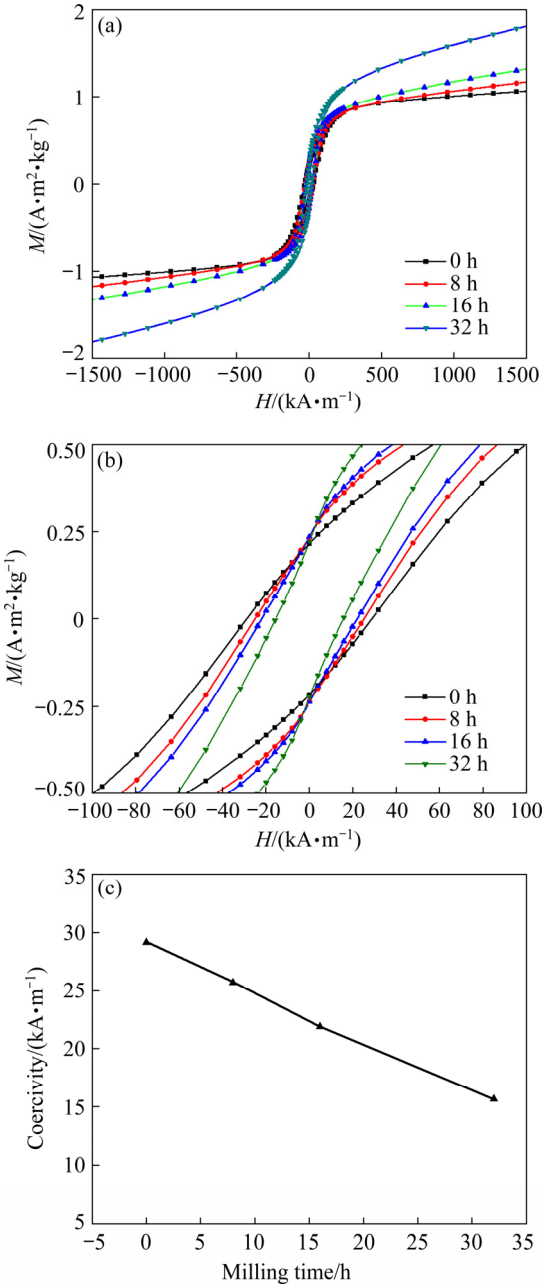

Fig. 5 Magnetization versus applied magnetic field strength (*M*−*H*) curves for mechanically milled FeAs for various durations, conducted at 77 K (a, b), and coercivity of FeAs with milling time from 0 to 32 h (c)

magnetic state transition temperatures at around 39.1 and 106.0 K for FeAs particles before ball grinding. Under the effect of ball milling, the magnetic state transition temperatures get close to each other gradually until the time of 32 h with only one transition temperature of T_N=57.0 K. This could be caused by the homogenization of the structural magnetic transition temperature, which means that the milled particles have more uniform structural characteristics than the raw FeAs particles.

As shown in Fig. 7, the Mössbauer spectra present a doublet which is assigned to paramagnetic Fe atoms in FeAs. Elemental Fe in the zero oxidation state typically shows a ferromagnetic characteristic peak of sextet, which is not observed in FeAs particles. However, it is not common that the FeAs particles with remarkable paramagnetic characteristics show good magnetization on M−H curves. In addition to the above discussion about the influence of lattice parameter, there is another reasonable speculation that the good magnetization might also be associated with the emergence of

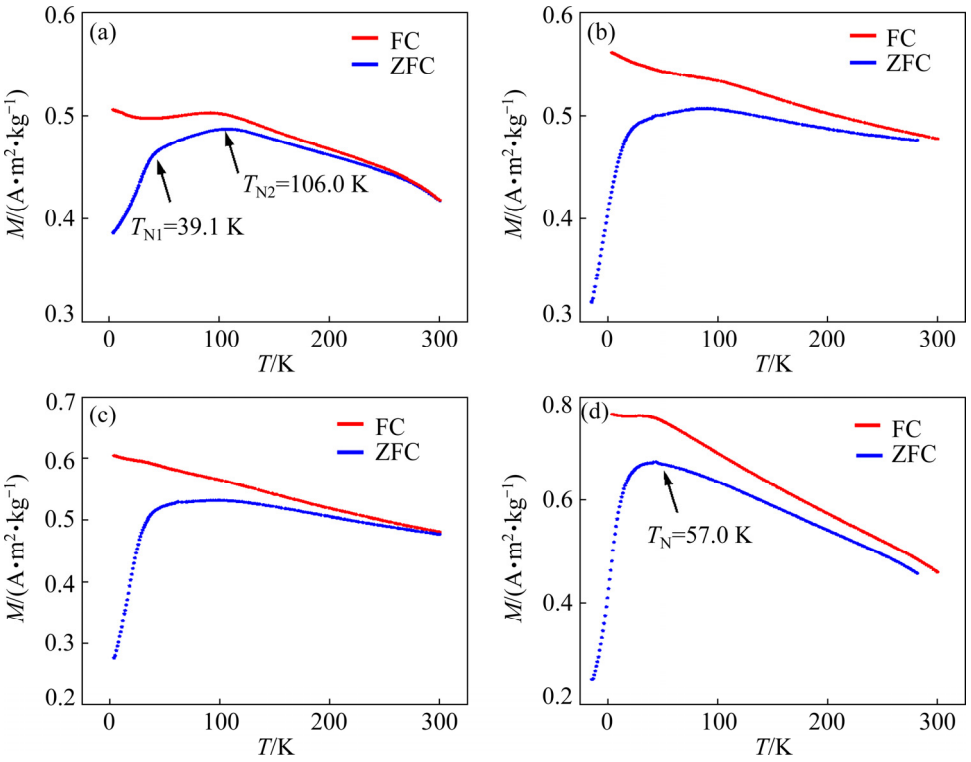

Fig. 6 Temperature dependences of magnetization under magnetic field strength H=79.6 kA/m for FeAs powders with various durations of ball milling: (a) 0 h; (b) 8 h; (c) 16 h; (d) 32 h

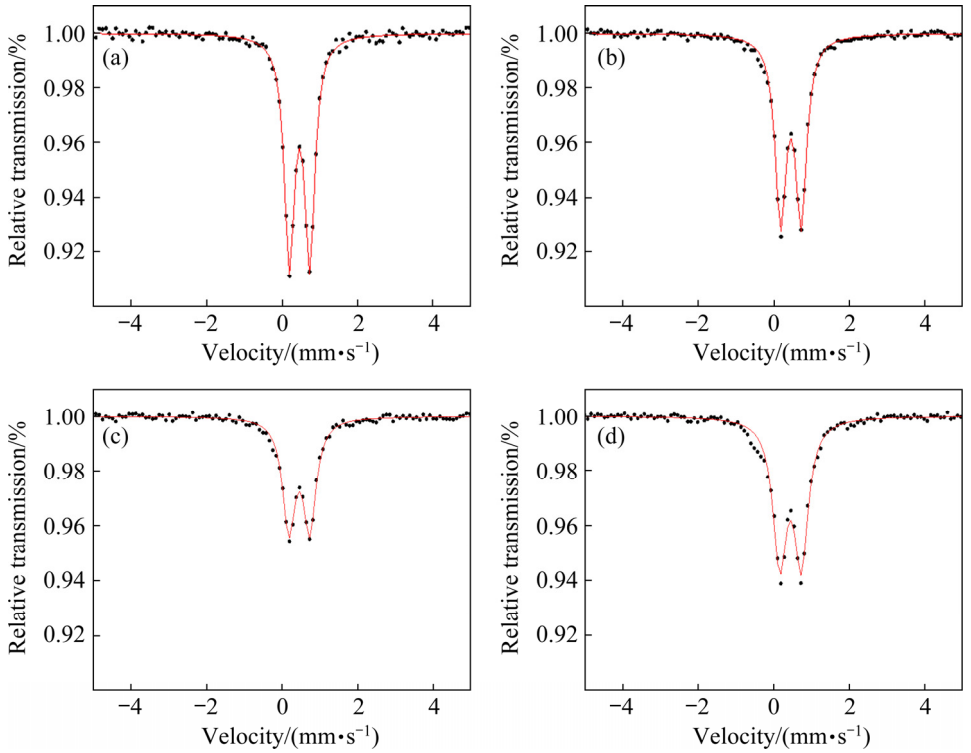

Fig. 7 Mössbauer spectra of FeAs particles collected at room temperature: (a) 0 h; (b) 8 h; (c) 16 h; (d) 32 h

superparamagnetic phase. The reduction of grain size in nanoscale, the decrease of coercivity, and the increase of magnetization along with ball milling provide strong supports for the emergence of superparamagnetic phase.

Details of Mössbauer spectral parameters are given in Table 2. The increase in the quadruple splitting with milling time is attributed to the gradual enhancement of lattice strain. The isomer shift of 0.45−0.47 mm/s and the quadruple splitting of 0.54−0.57 mm/s are consistent with those of bulk FeAs containing Fe in the oxidation state of +3. The increase of isomer shift can be caused by the increase of interatomic distance and the decrease of s-electron densities at Fe nuclei derived from ball milling [29]. The half-width at half-maximum of spectral line for FeAs without ball milling is about 0.16 mm/s. There is a distinct broadening of spectral lines over time of ball milling. The peak broadening is mainly due to the reduction of the grain sizes accompanied by high lattice strain, as a result of the increase of grain boundary density and defects in ball milling processing. Besides, The Mössbauer spectra collected from the series of FeAs particles show similar results compared with XRD in the analyses of microstructure changes and impurity detection. Thus, it has reason to rule out the presence of unreacted Fe impurity as well as any other oxidation states of Fe in these particles.

Table 2 Mössbauer spectral parameters fitted with least squares method for all FeAs samples at room temperature

Milling time/h	Isomer shift/ ($mm·s^{-1}$)	Quadruple splitting/($mm·s^{-1}$)	Half-width, ($\Gamma/2$)/($mm·s^{-1}$)
0	0.47	0.54	0.16
8	0.46	0.55	0.17
16	0.45	0.55	0.2
32	0.45	0.57	0.22

4 Conclusions

(1) Coarse-grain FeAs with high crystallinity can be obtained by high-energy ball milling and subsequent heat treatment.

(2) The mechanical force introduced by ball milling has significant influence on lattice parameters, grain size, and internal strain, but it does not change the FeAs phase. The lattice parameter of *b* and the internal strain increase gradually with milling time. The grain size can be reduced by high-energy ball milling, accompanied by the introduction of internal strains, forming FeAs particles with nanoscale grains and amorphous structure.

(3) The ball milling treatment has great influence on magnetic properties of nanocrystalline FeAs. The coercivity values are reduced from 29.2 to 15.6 kA/m, caused by the small grain size stemmed from ball milling. Apart from coercivity among magnetic properties, the high magnetization is attributed to the changes of lattice parameters and the emergence of superparamagnetic phase. Moreover, the ball milling process is advantageous to the homogenization of magnetic components.

Acknowledgments

The authors are grateful for the financial support from National Key Technologies R&D Program of China (No. 2018YFC1900302).

References

[1] KAMIHARA Y, WATANABE T, HIRANO M, HOSONO H. Iron-based layered superconductor La[$O_{1-x}F_x$]FeAs (x= 0.05−0.12) with T_C=26 K [J]. Journal of the American Chemical Society, 2008, 130: 3296−3297.

[2] GKOGKOSI E. *Ab initio* study on structural and electronic properties of ReOFeAs (Re: La, Sm, Nd, Ce, Gd) under hydrostatic pressure [J]. Journal of Physics Communications, 2019, 3: 1−10.

[3] MAISURADZE A, ZHIGADLO N D, LUETKENS H, AMATO A, KHASANOV R. Self-consistent two-gap approach in studying multi-band superconductivity of $NdFeAsO_{0.65}F_{0.35}$ [J]. Frontiers in Physics, 2020, 8: 1−11.

[4] HASE I, YANAGISAWA T. Effect of the distortion of FeX_4 (X=P, As) tetrahedron for the electronic structure of iron-pnictide system [J]. Physica C−Superconductivity and its Applications, 2010, 470: 538−542.

[5] CALAMIOTOU M, MARGIOLAKI I, GANTIS A, SIRANIDI E, REN Z A, ZHAO Z X, LIAROKAPIS E. Lattice anomalies in the $FeAs_4$ tetrahedra of the $NdFeAsO_{0.85}$ superconductor that disappear at T_C [J]. Europhysics Letters, 2010, 91: 57005.

[6] DESAI P, SONG K, KOZA J, PARITI A, NATH M. Soft-chemical synthetic route to superparamagnetic FeAs@C core-shell nanoparticles exhibiting high blocking temperature [J]. Chemistry of Materials, 2013, 25: 1510−1518.

[7] SELTE K, KJEKSHUS A. Structural and magnetic properties of FeP [J]. Acta Chemica Scandinavica, 1972, 26: 1276−1277.

[8] LYMAN P S, PREWITT C T. Room- and high-pressure crystal chemistry of CoAs and FeAs [J]. Acta Crystallographica, 1984, 40: 14−20.

[9] BLACHOWSKI A, RUEBENBAUER K, ZUKROWSKI J, BUKOWSKI Z. Magnetic anisotropy and lattice dynamics in

FeAs studied by Mössbauer spectroscopy [J]. Journal of Alloys and Compounds, 2014, 582: 167−176.
[10] SELTE K, KJEKSHUS A. The crystal structure of FeAs [J]. Acta Chemica Scandinavica, 1969, 23: 2047−2054.
[11] SELTE K, KJEKSHUS A, ANDRESEN A F. Magnetic structure and properties of FeAs [J]. Acta Chemica Scandinavica, 1972, 26: 3101−3113.
[12] JEFFRIES J R, BUTCH N P, CYNN H, SAHA S R, KIRSHENBAUM K, WEIR S T, VOHRA Y K, PAGLIONE J. Interplay between magnetism, structure, and strong electron-phonon coupling in binary FeAs under pressure [J]. Physical Review B, 2011, 83: 134520.
[13] RODRIGUEZ E E, STOCK C, KRYCKA K L, MAJKRZAK C F, ZAJDEL P, KIRSHENBAUM K, BUTCH N P, SAHA S R, PAGLIONE J, GREEN M A. Noncollinear spin−density−wave antiferromagnetism in FeAs [J]. Physical Review B, 2011, 83: 4400−4408.
[14] ZHAO Yong-hao, SHENG Hong-wei, LU Ke. Microstructure evolution and thermal properties in nanocrystalline Fe during mechanical attrition [J]. Acta Materialia, 2001, 49: 365−375.
[15] LEI Ruo-shan, WANG Ming-pu, GUO Ming-xing, LI Zhou, DONG Qi-yi. Microstructure evolution in nanocrystalline Cu−Nb alloy during mechanical alloying [J]. Transactions of Nonferrous Metals Society of China, 2007, 17: 603−607.
[16] AGUILAR C, PIO E, MEDINA J, PARRA C, MANGALARAJA R, MARTIN P, ALFONSO I, TELLO K. Effect of Sn on synthesis of nanocrystalline Ti-based alloy with fcc structure [J]. Transactions of Nonferrous Metals Society of China, 2020, 30: 2119−2131.
[17] TAI Zhong-zhi, LIU Wen-sheng, TANG Jian-cheng, MA Yun-zhu, ZHOU Ke-chao, HUANG Bai-yun. Nano-crystallization and soft magnetic properties of amorphous $Fe_{86}Zr_7B_6Cu_1$ ribbons annealed by hot isothermal pressing [J]. Journal of Central South University (Science and Technology), 2010, 41: 460−464. (in Chinese)
[18] MAHDAVI S, ALLAHKARAM S R. Effect of bath composition and pulse electrodeposition condition on characteristics and microhardness of cobalt coatings [J]. Transactions of Nonferrous Metals Society of China, 2018, 28: 2017−2027.
[19] HESSE J, RUBARTSCH A. Model independent evaluation of overlapped Mössbauer spectra [J]. Journal of Physics E: Scientific Instruments, 1974, 7: 526−532.
[20] CAMPILLO G, OSORIO J, ARNACHE O, GIL A, BELTRÁN J J, DORKIS L. Grain size reduction effect on structural and magnetic properties in $La_{1-x}Sr_xMnO_3$ (x=0.3, 0.4) by mechanical ball milling [J]. Journal of Physics Conference Series, 2019, 1247: 012015.
[21] ZUO Wen-liang, ZHANG Ming, NIU E, SHAO Xiao-ping, HU Feng-xia, SUN Ji-rong, SHEN Bao-gen. The coercivity mechanism of Pr−Fe−B nanoflakes prepared by surfactant-assisted ball milling [J]. Journal of Magnetism and Magnetic Materials, 2015, 390: 15−19.
[22] BLÁZQUEZ J S, IPUS J J, MORENO-RAMÍREZ L M, ÁLVAREZ-GÓMEZ J M, SÁNCHEZ-JIMÉNEZ D, LOZANO-PÉREZ S, FRANCO V, CONDE A. Ball milling as a way to produce magnetic and magnetocaloric materials: A review [J]. Journal of Materials Science, 2017, 52: 11834−11850.
[23] CHINNASAMY C N, NARAYANASAMY A, PONPANDIAN N, CHATTOPADHYAY K, SARAVANAKUMAR M. Order-disorder studies and magnetic properties of mechanically alloyed nanocrystalline Ni_3Fe alloy [J]. Materials Science and Engineering A, 2001, 304: 408−412.
[24] RIETVELD H M. A profile refinement method for nuclear and magnetic structures [J]. Journal of Applied Crystallography, 1969, 2: 65−71.
[25] HERZER G. Modern soft magnets: Amorphous and nanocrystalline materials [J]. Acta Materialia, 2013, 61: 718−734.
[26] RONDINONE A J, SAMIA A C S, ZHANG Z J. Superparamagnetic relaxation and magnetic anisotropy energy distribution in $CoFe_2O_4$ spinel ferrite nanocrystallites [J]. Journal of Physical Chemistry B, 1999, 103: 6876−6880.
[27] LUO Wei-li, NAGEL S R, ROSENBAUM T F, ROSENSWEIG R E. Dipole interactions with random anisotropy in a frozen ferrofluid [J]. Physical Review Letters, 1991, 67: 2721−2724.
[28] REIMERS J N, DAHN J R, GREEDAN J E, STAGER C V, SACKEN U V. Spin glass behavior in the frustrated antiferromagnetic $LiNiO_2$ [J]. Journal of Solid State Chemistry, 1993, 102: 542−552.
[29] LI F S, WANG L, WANG J B, ZHOU Q G, ZHOU X Z, KUNKEL H P, WILLIAMS G. Site preference of Fe in nanoparticles of $ZnFe_2O_4$ [J]. Journal of Magnetism and Magnetic Materials, 2004, 268: 332−339.

粗晶和纳米晶 FeAs 的微观结构与磁学性能

周 元[1]，王云燕[1,2]，梁彦杰[1,2]，周艺伟[1]，刘振兴[1]，彭 聪[1,2]，柯 勇[1,2]，闵小波[1,2]

1. 中南大学 冶金与环境学院，长沙 410083；2. 国家重金属污染防治工程技术研究中心，长沙 410083

摘 要：研究粗晶及纳米晶 FeAs 的微观结构和磁学性能。首先通过高能球磨和热处理制备粗晶 FeAs，随后将粗晶 FeAs 进行不同时间球磨得到纳米晶 FeAs。结果表明，球磨时间为 32 h 时，平均晶粒尺寸由>100 nm 减小到 32.4 nm，同时内应变增加到 0.568%。随着球磨时间的增加，矫顽力由球磨前的 29.2 kA/m 降低到 15.6 kA/m，同时磁化强度提高。分析认为，晶粒尺寸的减小导致 FeAs 矫顽力的降低，而球磨过程中晶胞参数的变化和超顺磁相的出现则导致磁化强度的提高。

关键词：高能球磨；砷化铁；矫顽力；磁化强度

(Edited by Bing YANG)